Desalination and Water Treatment
www.deswater.com

doi: 10.5004/dwt.2018.21733

101 (2018) 268–282
January

Recovery of vanadium–EDTA complex from extraction leachate of vanadium secondary resources: optimization and experimental investigation

Mohammad Poorbaba, Mansooreh Soleimani*

Department of Chemical Engineering, Amirkabir University of Technology, No. 424, Hafez Ave., Tehran, Iran, Tel./Fax: + 98 (21) 66405847; emails: soleimanim@aut.ac.ir (M. Soleimani), m.pourbaba@aut.ac.ir (M. Poorbaba)

Received 7 July 2017; Accepted 26 November 2017

ABSTRACT

It is imperative to recover vanadium from secondary resources due to its non-biodegradability, toxicity and economical benefits. An aqueous solution of ethylenediaminetetraacetic acid (EDTA) can facilitate vanadium extraction from secondary resources. The goal of this paper is V-EDTA complex recovery from an aqueous phase by utilizing commercial activated carbon. The central composite design was chosen to study and optimize the main operating parameters including initial vanadium concentration ($C_{i,V}$), EDTA to vanadium molar ratio (L/M), initial solution pH (pH_i) and adsorbent dosage ($C_{Ads.}$). Based on analysis of variance, the non-complete cubic model of V-EDTA recovery was highly significant due to its probability value (<0.0001). Based on the derived model, the optimum operating conditions were: $C_{i,V}$ = 40 mg L^{-1}, L/M = 3, pH_i = 2 and $C_{Ads.}$ = 12 g L^{-1}; and the maximum vanadium recovery percentage was 98.25. To investigate the process mechanism, the adsorption of free EDTA and Na was also studied. The kinetic results indicated that the recovery process follows a pseudo-second-order kinetic model. The Freundlich and Dubinin–Radushkevich isotherms were able to adequately describe the equilibrium data. The thermodynamic parameters indicated that this process was spontaneous, feasible and possessed an exothermic nature.

Keywords: Recovery; Vanadium; Ethylenediaminetetraacetic acid; Activated carbon; Optimization

1. Introduction

Heavy metals could cause serious problems to the environment and living organisms due to their non-biodegradability [1,2]. They can be released to the environment through effluents of industries such as metal plating and mining [3,4]. Vanadium is a heavy metal that presents environmental toxicity concerns [5] as well as useful applications in different industries such as steel, metallurgy, glass, ceramic, textile, photography and pigments manufacturing [6–8]. Therefore, it is necessary to recover and reduce this heavy metal to its standard limits [9].

Vanadium is produced from primary and secondary resources. Heavy cuts of crude oil [10], spent catalysts [11–13] and fly ash produced in heavy fuel power plants [14] are just some of the secondary vanadium resources to mention. Extraction, membrane, adsorption and distillation are some of the noteworthy separation techniques that can be used to recover vanadium from its resources [10]. The point of interest in this paper was the extraction method. Compared with inorganic acids, the extraction processes with organic acids are more desirable due to their ability to form a metal–ligand complex at more favorable operating conditions [15].

Ethylenediaminetetraacetic acid (EDTA) is a very useful organic acid and strong chelating agent that has been used to extract vanadium and other heavy metals from secondary resources [10,14–16]. The V-EDTA complex is formed and remains in the extractant phase, after the extraction process is applied with an EDTA aqueous solution. Due to the benefits such as low cost, flexibility and ease of operation offered by adsorption processes [6], the point of concern in this paper was to recover the V-EDTA complex from the extractant phase via an adsorption method. Among different adsorbents that

* Corresponding author.

have been used to adsorb vanadium ions such as silica, activated carbon, bentonite clay, zeolite, chitosan and their functionalized types [17–19], the activated carbon was chosen for its favorable properties and better efficiency in adsorbing organic compounds [20–23].

Our survey of the relevant published papers has indicated that our study of V-EDTA adsorption from aqueous phase on activated carbon is the first investigation of its kind. By applying the response surface method (RSM), a model was obtained to navigate the design space based on the operating parameters.

The main objectives of the present study include the following tasks:

- Study and optimize the main parameters influencing V-EDTA recovery including initial vanadium concentration, EDTA concentration, initial pH of the solution and adsorbent dosage.
- Obtain an accurate model for the V-EDTA recovery based on operational conditions using central composite design (CCD).
- Study the kinetics and isotherms of V-EDTA adsorption and describe them by a proper model.
- Investigate the recovery process mechanism by studying the adsorption of other components including free EDTA and Na.

2. Materials and experimental methods

2.1. Chemicals

The adsorbent used in this study was a commercial activated carbon based on selected grades of coal produced by steam activation. This carbon is produced by CABOT Company (China) (GAC 830W), and was named NAC in this paper. V_2O_5 and $C_{10}H_{14}N_2Na_2O_8.2H_2O$ were used to prepare the stock solutions of V-EDTA complex. The initial pH of the V-EDTA complex solutions was adjusted by diluted NaOH and HNO_3. $ZnCl_2$ and xylenol orange (XO) indicators were used to determine the presence of free EDTA in the solutions. All solutions were prepared with deionized water and ultra pure grade chemicals from Merck Company (Germany).

2.2. Characterization of adsorbent

An NAC characterization was performed for selected physical and chemical properties by applying the standard test methods (ASTM). The effective particle size, iodine number, apparent density, ball-pan hardness, pH_{pzc} and porous texture of NAC were also determined.

The NAC porous texture was studied by applying N_2 adsorption at 77 K (Brunauer-Emmett-Teller method) [24]. The specific surface area, average pore radius and pore volume were determined before and after the adsorption process by the BEL Belsorp-mini instrument. The NAC surface functional groups were studied before and after the process, by studying the Fourier-transform infrared (FTIR) spectrum within a 400–4,000 range by a NEXUS Nicolet 670 instrument.

To measure the pH_{pzc} (point of zero charge) of NAC, several 0.1 N NaCl solutions whose initial pHs were adjusted with HNO_3 or NaOH, were prepared. Then, 50 mg of NAC was added to 50 mL of each of the 0.1 N NaCl solutions. After that, the mixtures were agitated on a shaker incubator at room temperature for 24 h. Finally, after filtering the adsorbents, the final pH of the solutions was determined and compared with the initial pH. If the initial pH equals the final pH after reaching equilibrium, that pH is the pH_{pzc} [25].

2.3. Metal–ligand solutions preparation

To prepare a stock solution of V-EDTA from vanadium with a concentration of 2,000 mg L^{-1}, the EDTA disodium salt and vanadium pentoxide salt were weighed and dissolved in deionized water in an appropriate volumetric flask. After that, the flask was placed in a water bath with a temperature of 35°C–37°C for 24 h. Then, the mixture was agitated at 250 rpm for at least 3 h. It could then be claimed that the V-EDTA complex had been fully formed. The stock solution was diluted with deionized water to a certain concentration for each one of the experiments.

2.4. Experimental procedures

The RSM was used to design experiments to investigate V-EDTA adsorption on NAC. The influences of vanadium concentration, EDTA concentration, initial pH of the solution and adsorbent dosage on the process were studied. To perform each experiment, 50 mL of the solution containing V-EDTA was prepared, and the pH of the solution was adjusted by diluted HNO_3 or NaOH. A pH meter with a degree of accuracy of 0.1 was used to determine the pH of the solution (Genway, model 3345). After adding the adsorbent, the mixture was agitated in a shaker incubator (N-BIOTEK, model NB-205) at 230 rpm for 4 h and at a constant temperature of 25°C. Afterwards, the mixture was filtered by Whatman no. 1 filter papers. Finally, vanadium concentration was determined by the inductively coupled plasma optical emission spectrometry (ICP-OES) (Varian, model 730-ES Axial) analysis instrument. The vanadium recovery percentage was calculated by Eq. (1):

$$\text{Vanadium recovery } \% = \frac{C_{i,\text{V}} - C_{f,\text{V}}}{C_{i,\text{V}}} \times 100 \quad (1)$$

where $C_{i,V}$ and $C_{f,V}$ are the initial and final concentration of vanadium (mg L^{-1}), respectively.

Since the EDTA concentration was one of the operating parameters and complex of V-EDTA that is 1:1, it means that 1 mol of each vanadium and EDTA was required to form a 1 mol of V-EDTA complex [26], and free EDTA could be found in the solution of some experiments. Also, sodium concentration varies by changing the EDTA concentration. In order to study the V-EDTA recovery mechanism, the free EDTA and sodium concentrations were measured before and after the process in some of the experiments (at star points marked in Table 4). A Flame photometer (Sherwood, model 410) was used to measure the sodium concentration. The sodium adsorption percentage was calculated by Eq. (2):

$$\text{Na adsorption } \% = \frac{C_{i,\text{Na}} - C_{f,\text{Na}}}{C_{i,\text{Na}}} \times 100 \quad (2)$$

where $C_{i,Na}$ and $C_{f,Na}$ represent the concentrations (mmol L^{-1}) before and after the adsorption process.

The free EDTA concentration was calculated by a titration technique with 0.001 M $ZnCl_2$ solution [27]. Additionally, an XO indicator and a buffer solution with a pH of 5.5 were used successively, to recognize the titration end point and keep solution pH constant. The titration was ended when the initial yellow color of the solution turned into purple-red. The purple-red color was generated as a result of Zn–XO complex formation. The free EDTA adsorption percentage was determined by Eq. (3).

$$\text{Free EDTA adsorption \%} = \frac{C_{i,\text{EDTA}} - C_{f,\text{EDTA}}}{C_{i,\text{EDTA}}} \times 100 \quad (3)$$

where $C_{i,EDTA}$ and $C_{f,EDTA}$ are the free EDTA concentrations (mmol L^{-1}) at the initial and final points of the process.

2.5. RSM experimental design

The statistical design of experiments (DOE) is one of the principal tools in researches carried out in laboratories and industries. These designs allow researchers to obtain reliable results, save time, make significant reductions in the number of experiments and ultimately optimize the process [28]. In the RSM, the statistical and mathematical techniques are combined. This combination incorporates the usefulness of the RSM method to optimize a process in which several factors have complex interactions [28–31].

In this paper, the recovery experiments were designed by a commercial DOE software called Design Expert (version 8.0.6) from Stat-Ease Company (Minneapolis, USA). In Design Expert, CCD was chosen for its numerous benefits such as great ability to estimate the quadratic model, insensitivity to missing data and replicating the center point for higher prediction accuracy.

By varying a parameter in CCD called alpha (α), different CCDs such as rotatable, spherical, orthogonal quadratic, practical and face centered will be obtained. Each of these designs deliver different star points locations. In this work, the face centered CCD ($\alpha = 1$) was chosen due to the limitation of initial operating pH factor occurring at other CCD designs.

In accordance with our preliminary investigation, four operating factors were selected as independent variables. They are vanadium concentration (X_1), EDTA to vanadium molar concentration ratio called L/M (X_2), initial pH (X_3) and adsorbent dosage (X_4). As a quest for better physical justification, the EDTA concentration was defined as the L/M ratio, which is an equivalent representation. Table 1 represents the ranges of the four independent factors and the corresponding coded levels. Generally, there are five coded levels in a CCD that include $-\alpha$, –1, 0, +1 and $+\alpha$. However, the number of coded levels was reduced to three by considering a face centered design.

The relationship between vanadium recovery percentage as the response factor, and the independent variables was established by applying the face centered CCD. Moreover, the obtained model was utilized to maximize the response, and the optimum values of the variables were also defined.

Designing the experiments by face centered CCD, resulted in 30 experiments. The number of experiments is obtained from the following relation: $2^K + 2K + 6$, where K is the number of independent variables [31].

Table 1
Ranges and levels of independent factors

Factors	Coded levels		
	–1	0	+1
X_1: Vanadium concentration (mg L^{-1})	40	120	200
X_2: L/M	1	2	3
X_3: Initial pH	2	5	8
X_4: Adsorbent dosage (g L^{-1})	2	7	12

To obtain the maximum vanadium recovery percentage, and determine the optimum operating factors, a regression model was solved [32]. Linear, quadratic and cubic models were tested to describe the vanadium recovery as a function of the independent variables. These models are illustrated in Eqs. (4)–(6), respectively [33]:

$$y = \beta_0 + \sum_{i=1}^{4} \beta_i X_i \quad (4)$$

$$y = \beta_0 + \sum_{i=1}^{4} \beta_i X_i + \sum_{i=1}^{3} \sum_{j=i+1}^{4} \beta_{ij} X_i X_j + \sum_{i=1}^{4} \beta_{ii} X_i^2 \quad (5)$$

$$y = \beta_0 + \sum_{i=1}^{4} \beta_i X_i + \sum_{i=1}^{3} \sum_{j=i+1}^{4} \beta_{ij} X_i X_j + \sum_{i=1}^{4} \beta_{ii} X_{i_i}^2 + \sum_{i=1}^{2} \sum_{j=i+1}^{3} \sum_{k=i+2}^{4} \beta_{ijk} X_i X_j X_k + \sum_{i=1}^{4} \sum_{j=1, j^1 i}^{4} \beta_{ij} X_i X_j^2 + \sum_{i=1}^{4} \beta_{iii} X_i^3 \quad (6)$$

where i, j and k are the index numbers for the patterns and y is the response (vanadium recovery percentage). β_0 is the regression coefficient term, and β_i, β_{ii} and β_{iii} indicate linear, squared and cubic effects of the models, respectively. β_{ij} is the interaction effect for the quadratic model, and β_{ijk} and β_{ijj} likewise are the interaction effects for the square and cubic models, and X_i, X_j and X_k are the coded independent factors.

The proper model was selected in accordance with the diagnostic plots and model constants that include correlation coefficients, adequate precision and coefficient of variation (CV %). These constants are used to examine the model's quality and accuracy. Also, the selected model constants were optimized by analysis of variance (ANOVA).

Three correlation coefficients namely R^2, adjusted R^2 and predicted R^2 were used to identify the best model. The correlation coefficients of the best model which can be used to navigate the design space are close to one, and the values of adjusted R^2 and predicted R^2 are in reasonable agreement with each other. Also, adequate precision, which demonstrates the signal to noise ratio and CV % that expresses the precision and repeatability of the results were studied to choose the proper model. Moreover, by using ANOVA, and taking into account the F value (Fisher variation ratio) and probability value (Prob > F), the selected model was modified and improved to achieve a better description of the experimental data [28,31,33].

2.6. Kinetics studies

To investigate the V-EDTA adsorption process kinetics, 50 mL of its solution was contacted with the adsorbent at different time steps spanning 10–1,860 min. A 200 mg L^{-1} of vanadium solution was prepared for the test. Other operating parameters (L/M ratio, initial solution pH and adsorbent dosage) were set at their RSM optimum values. The temperature was ambient and the mixture was agitated at 230 rpm. After each time step, the adsorbent was separated by filtration and the vanadium concentration in the residual solution was determined. The amount of adsorbed vanadium after each time step, q_t (mg g^{-1}), can be obtained from Eq. (7):

$$q_t = \frac{C_{i,V} - C_{f,V}}{C_{Ads.}} \tag{7}$$

where $C_{i,V}$ is the initial vanadium concentration (mg L^{-1}), $C_{t,V}$ is its concentration at time t (min) in mg L^{-1} and $C_{Ads.}$ is the adsorbent dosage (g L^{-1}).

2.7. Equilibrium studies

The equilibrium studies were carried out at different initial concentrations of vanadium (100–320 mg L^{-1}). The other operating conditions were set in accordance with the optimum conditions derived from the RSM analysis. The equilibrium tests were carried out by contacting 50 mL of V-EDTA solution with the adsorbent at three temperatures (25°C, 35°C and 45°C). The mixture was agitated in an orbital shaker incubator at 230 rpm for 31 h to reach equilibrium. Finally, the mixture was filtered and the solution was introduced to ICP-OES to determine the vanadium concentration. Eq. (8) was used to calculate q_e (mg g^{-1}), the amount of adsorbed vanadium.

$$q_e = \frac{C_{i,V} - C_{e,V}}{C_{Ads.}} \tag{8}$$

where $C_{i,V}$ and $C_{e,V}$ are vanadium concentrations at the initial and equilibrium (mg L^{-1}).

3. Results and discussions

3.1. Characteristics of adsorbent

The NAC characteristics are listed in Table 2, and its size distribution is presented in Table 3. The NAC porous texture including total surface area, mean pore diameter and total pore volume was measured before and after the recovery process. The values before the process are reported in Table 2, while the values after the recovery process for the maximized adsorbent capacity are as follows:

Total surface area = 846.7 m^2 g^{-1}, mean pore diameter = 2.141 nm and total pore volume = 0.453 cm^3 g^{-1}. Due to an increase of the mean pore diameter and decrease of total pore volume, it can be concluded that the V-EDTA complex adsorption could occur at micropores.

To identify NAC functional groups, an FTIR spectroscopy was performed. The results before and after the adsorption are shown in Fig. 1. Before the adsorption, the wide peak

Table 2
Characteristics of the NAC adsorbent

Parameter	Value	Measurement method
Effective particle size (mm)	1.6	–
Iodine number (mg I_2 g^{-1})	950	ASTM D4607-14
Apparent density (g mL^{-1})	0.47	ASTM D2854-09
Ball-pan hardness (%)	95	ASTM D3802-16
pH_{pzc}	8.3	–
Total surface area (m^2 g^{-1})	1021.5	–
Mean pore diameter (nm)	2.073	
Total pore volume (cm^3 g^{-1})	0.529	

Table 3
Particle size distribution of NAC adsorbent

Mesh no.	Mesh size (μm)	Weight passed through (%)	Measurement method
10	2,000	76.83	Mesh sieve
12	1,680	52.33	
14	1,410	9.95	
20	840	0.68	

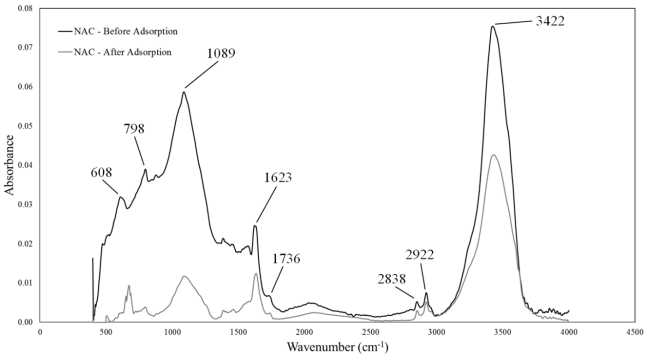

Fig. 1. FTIR spectra of NAC before and after V-EDTA adsorption.

at 3,422 cm^{-1} is attributed to the O–H functional group. The C–O strong peak at 1,089 cm^{-1} proves that the identified O–H is attributed to alcohols or phenols [34]. The peaks between 2,850 and 3,000 cm^{-1} may be attributed to C–H stretching in an alkane [34]. The existing probabilities of N–H bending for primary and secondary amides are observed at a peak of 1,623 cm^{-1} [34]. Also, the moderate peaks at 1,300–1,600 cm^{-1} might be attributed to C–H bending in the form of $–CH_2–$ and $–CH_3$ in an alkane [34]. The peak at 798 cm^{-1} is probably attributed to a rocking C–H bending in an alkane or aromatic [34]. After the adsorption process, the intensity of O–H and C–O peaks decreased severely. This shows that OH^- is separated from the NAC surface during the adsorption process. By releasing OH^-, the proper conditions for adsorption of the currently negatively charged V-EDTA complex are provided [26]. However, the pH of the solution increased, and the pH measurements verify this fact. The pH increase for each experiment is shown in Table 4.

Table 4
CCD experiments and the corresponding results

Run	Independent variables				Vanadium recovery %	Final pH	Comment
	X_1	X_2	X_3	X_4			
	$C_{i,V}$ (mg L^{-1})	L/M	Initial pH	$C_{Ads.}$ (g L^{-1})			
1	40.00	1.00	2.00	2.00	35.08	2.10	FP
2	200.00	3.00	8.00	12.00	6.61	8.00	FP
3	120.00	3.00	5.00	7.00	17.42	6.80	SP
4	200.00	3.00	2.00	12.00	55.30	2.10	FP
5	120.00	2.00	2.00	7.00	50.82	2.10	SP
6	40.00	3.00	8.00	2.00	9.25	7.50	FP
7	200.00	1.00	2.00	12.00	69.04	2.30	FP
8	200.00	1.00	2.00	2.00	16.83	2.10	FP
9	120.00	2.00	5.00	7.00	15.57	6.80	CP
10	120.00	2.00	8.00	7.00	3.94	8.10	SP
11	120.00	2.00	5.00	7.00	12.83	7.00	CP
12	40.00	3.00	2.00	12.00	98.25	2.20	FP
13	200.00	3.00	2.00	2.00	9.88	2.00	FP
14	120.00	2.00	5.00	2.00	2.19	6.40	SP
15	40.00	3.00	2.00	2.00	35.21	2.00	FP
16	120.00	2.00	5.00	7.00	22.78	6.70	CP
17	120.00	1.00	5.00	7.00	12.07	7.30	SP
18	120.00	2.00	5.00	7.00	17.75	6.80	CP
19	120.00	2.00	5.00	7.00	16.03	6.80	CP
20	120.00	2.00	5.00	12.00	19.69	7.00	SP
21	40.00	1.00	8.00	2.00	12.67	7.40	FP
22	40.00	1.00	8.00	12.00	43.17	7.80	FP
23	200.00	1.00	8.00	12.00	12.57	8.10	FP
24	200.00	3.00	8.00	2.00	0.69	7.70	FP
25	40.00	2.00	5.00	7.00	36.04	7.20	SP
26	40.00	3.00	8.00	12.00	38.08	8.00	FP
27	200.00	1.00	8.00	2.00	2.13	7.60	FP
28	120.00	2.00	5.00	7.00	15.82	6.80	CP
29	200.00	2.00	5.00	7.00	12.63	6.90	SP
30	40.00	1.00	2.00	12.00	76.71	2.10	FP

FP, factorial point; SP, star point; CP, central point.

The pH increase is a function of the L/M ratio, initial pH and adsorbent dosage. Considering the NAC at 8.3, there was a tendency originating from the adsorbents that could increase the solution pH. By increasing the NAC dosage, the tendency would be greater to increase the solution pH. However, the other parameters such as the L/M ratio and the initial pH have affected this tendency. It means that, when the initial solution pH was set at 2.00, a slight pH increase was realized at the end of the adsorption process. It was observed at this initial pH, that the solution had a buffered-like behavior. This behavior was observed again, when the initial pH was near pH_{pzc} (8.00). At L/M greater than 1, there was free EDTA in the solution which made the solution more acidic. Also, the EDTA adsorption occurred along with V-EDTA adsorption. So, the EDTA removal from the solution resulted in changes of the solution pH.

3.2. RSM and model analysis

According to the RSM design, 30 experiments were carried out to study the effects of selected parameters on V-EDTA recovery. The operating conditions for each experiment and the obtained results are reported in Table 4. Based on the obtained results (Table 4), the maximum vanadium recovery percentage was 98.25 that occurred in run 12 at $C_{i,V}$ = 40 mg L^{-1}, L/M = 3.00, pH_i = 2.00 and $C_{Ads.}$ = 12 g L^{-1}. Moreover, the minimum vanadium recovery percentage was 0.69% observed in run 24, and obtained at $C_{i,V}$ = 200.00 mg L^{-1}, L/M = 3.00, pH_i = 8.00 and $C_{Ads.}$ = 2.00 g L^{-1}.

An ANOVA was performed to determine the model that can best predict the experimental data. A statistical analysis was carried out for each regression parameter to identify the importance of each source in the final model. This identification was achieved by observing the *F* value and

Prob > *F* of each source, which demonstrates their effectiveness and importance. At the ANOVA table, the sources having Prob > *F* less than 0.0500 are significant model terms, and those whose Prob > *F* are greater than 0.1000 are not significant, and could be omitted to improve model quality and accuracy [35]. The ANOVA for the vanadium recovery percentage is shown in Table 5. According to this table, the model *F* value and Prob > *F* parameters are 62.20 and <0.0001, respectively. These two values indicate the significance of the obtained model.

Based on the ANOVA table and Prob > *F* criteria for each source, X_1, X_3, X_4, X_1X_2, X_3X_4, X_1^2, X_3^2, X_4^2 and $X_1^2X_3$ are the significant model terms. However, there are three non-significant terms in the final model that were not omitted. One of them is the main source term X_2, and the other two are interaction terms X_1X_3 and $X_1^2X_2$. It was observed that the adequacy of the model improved with the presence of the abovementioned three terms. The final model in terms of the substituted operating parameters is presented in Eq. (9).

$$\begin{aligned}\text{Sqrt (Vanadium recovery \%)} = {} & 7.13609 - 0.025156X_1 \\ & - 0.53983X_2 - 0.80514X_3 + 0.85083X_4 + 0.017699X_1X_2 \\ & - 0.012893X_1X_3 - 0.022273X_3X_4 + 8.66900E{-}05X_1^2 \\ & + 0.093065X_3^2 - 0.030409X_4^2 - 8.57244E{-}05X_1^2X_2 \\ & + 5.00295E{-}05X_1^2X_3 \end{aligned} \quad (9)$$

As is obvious in Eq. (9), the square root of the vanadium recovery percentage is used as a response instead of its ordinary form. In cases in which the ratio of maximum to minimum response is greater than 10, a transformation usually requires obtaining a proper model. The results (Table 4) indicate that the maximum to minimum response ratio is 142. Therefore, the square root transform was selected (Lambda = 0.5) based on Fig. 2, that represents the Box–Cox plot derived from Design Expert software.

Table 5
ANOVA table for V-EDTA recovery

Source	Sum of squares	Degrees of freedom	Mean square	*F* value	Prob > *F*
Model	139.09	12	11.59	62.20	<0.0001
X_1	24.32	1	24.32	130.51	<0.0001
X_2	0.24	1	0.24	1.31	0.2679
X_3	13.22	1	13.22	70.97	<0.0001
X_4	44.29	1	44.29	237.71	<0.0001
X_1X_2	0.85	1	0.85	4.54	0.0480
X_1X_3	0.72	1	0.72	3.88	0.0653
X_3X_4	1.79	1	1.79	9.58	0.0066
X_1^2	3.18	1	3.18	17.07	0.0007
X_3^2	1.99	1	1.99	10.69	0.0045
X_4^2	1.64	1	1.64	8.80	0.0086
$X_1^2X_2$	0.54	1	0.54	2.87	0.1084
$X_1^2X_3$	1.64	1	1.64	8.80	0.0086
Residual	3.17	17	0.19	–	–
Lack of fit	2.39	12	0.20	1.28	0.4192
Pure error	0.78	5	0.16	–	–

Also, the model is a non-complete cubic model. The choice of a complete cubic model would have included some terms, that would be aliased with one another, and the least squares parameters for the model would also not be unique. Hence, using the complete cubic model was not possible. Therefore, to solve the problem and obtain an adequate model for the recovery process, the non-important terms were omitted and the non-complete cubic model was selected as the desirable model. Mehrabi et al. [31] have applied the RSM to develop a similar non-complete cubic model that optimizes nitrate removal from water by activated carbon.

The model's constants and specifications make it possible to evaluate the quality of the model and accuracy of its predicted values. The R^2 values assess the total variation of experimental data. Based on statistical analysis, the R^2, adjusted R^2 and predicted R^2 for the obtained model are 0.9777, 0.9620 and 0.8979, respectively. Based on the reasonable agreement and closeness of adjusted R^2 and predicted R^2 values, the model is acceptable in this context. Also, the lack of fitness of the model to the experimental data is tested by the lack of fit *F* value parameter (Table 5). The value 1.28 for this parameter shows that the lack of fitness of the model is not significant relative to the pure error. Moreover, the signal to noise ratio, which is measured by an adequate precision parameter, is 32.178 for the model. The values greater than 4 indicate an adequate signal [36,37]. Furthermore, the CV %) of 9.38% expresses the precision and repeatability of the predicted results. Generally, lower the CV %, higher the precision and repeatability.

The diagnostic plots are useful tools that ensure model accuracy and finalization. They could be helpful to check the normality of residuals, constant error, predicted values, etc. To compare the accuracy of the predicted values with the experimental data, a predicted vs. actual value plot was prepared. As can be seen in Fig. 3, passing a straight line through the plotted points indicates that the predicted and actual values are nearly the same. Also, Fig. 4 demonstrates the normal plot of the residuals, illustrating that the error terms are normally distributed. Therefore, the model statics and diagnostic plots show that the model obtained via the RSM, describes the design space accurately and favorably.

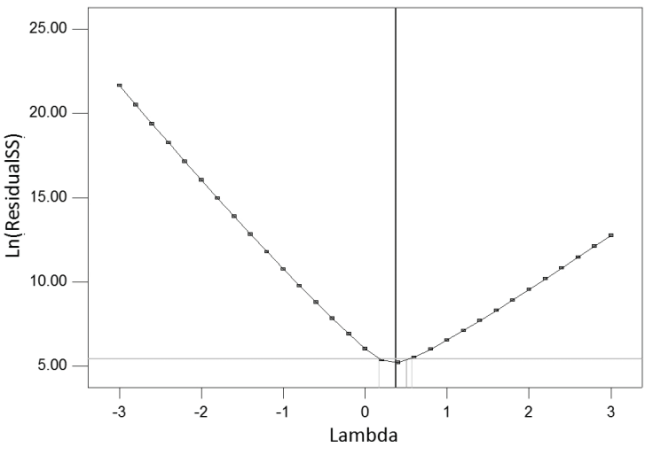

Fig. 2. Box–Cox plot for power transforms at the vanadium recovery percentage response.

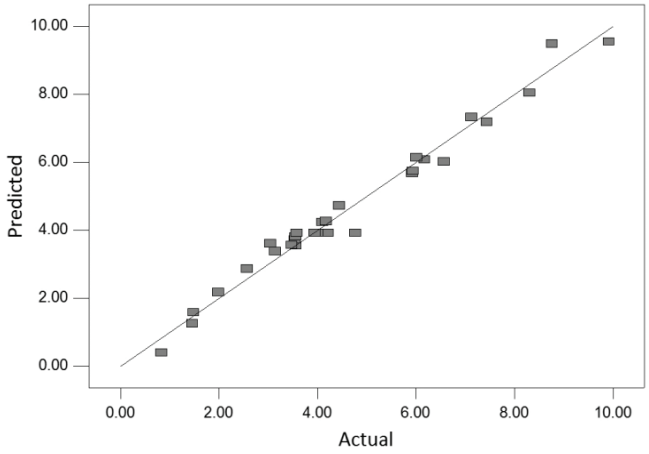

Fig. 3. Plot of predicted vs. actual values for vanadium recovery.

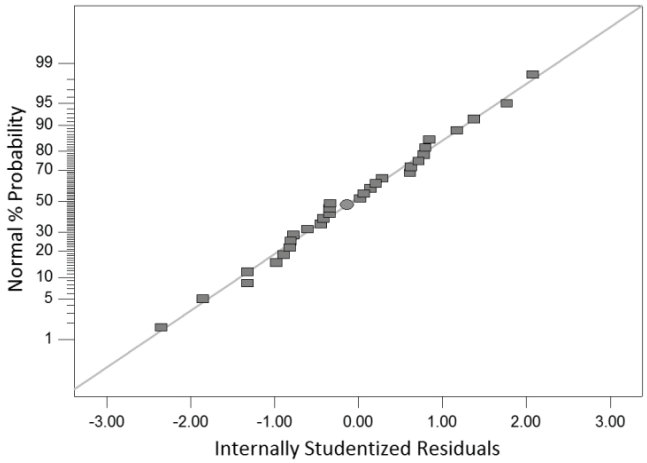

Fig. 4. Normal plot of residuals for vanadium recovery.

The perturbation plot was used to determine the most influential variable in the vanadium recovery process. As can be seen in Fig. 5, the initial pH (X_3) had the most influence on V-EDTA recovery because the slope of the initial pH curvature is greater than the other curvatures. This criterion also indicates that the L/M factor (X_2) had the least influence on the final response. The *F* value and Prob > *F* of L/M variable (Table 5) and its perturbation curvature lead to the conclusion that recovery of the V-EDTA complex does not depend on the L/M ratio or excess EDTA concentration.

3.3. Interaction effects of operating parameters

The paired interaction effects of operating parameters on the vanadium recovery percentage are illustrated in Fig. 6 as a 3D surface plots format. To generate these plots, two of the four operational factors were set to their optimum values, while the influences of the two remaining factors on the vanadium recovery percentage were investigated.

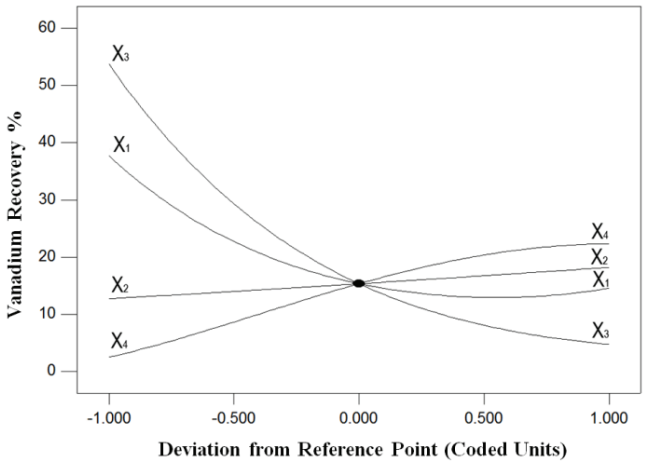

Fig. 5. Perturbation plot for V-EDTA recovery ($C_{i,V}$ = 120.00 mg L^{-1}, L/M = 2.00, pH_i = 5.00, $C_{Ads.}$ = 7.00 g L^{-1}).

3.3.1. Effect of vanadium concentration and adsorbent dosage

The effects of adsorbate concentration and adsorbent dosage are well known in the adsorption process. The initial vanadium concentration affects the adsorption driving force, and the amount of adsorbed vanadium (*q*) usually increases by increasing it. However, due to NAC active sites which are constant at a certain dosage, increasing the vanadium concentration results in decreasing the vanadium recovery percentage. Figs. 6(a) and (b) illustrate the initial vanadium concentration effect.

In most cases, there is a direct relationship between adsorbent dosage and adsorbate recovery percentage, due to the increase in the number of adsorbent active sites. In few cases, the effects such as adsorbent agglomeration or dissolution in the solution reduce the adsorption efficiency [18,38]. However, as is shown in Fig. 6(c), a direct relationship exists between adsorbent dosage and vanadium recovery percentage.

3.3.2. Effects of initial pH and L/M ratio

The perturbation plot (Fig. 5) indicated that the most important parameter in the vanadium recovery process was the initial pH of the solution. This parameter set the charge of the adsorbent surface as well as the V-EDTA complex. The surface charge of the NAC is positive when the solution pH is lower than its pH_{pzc}. As the solution pH decreases, the NAC surface charge becomes stronger, and its ability to adsorb anions is improved. Moreover, the species distribution of the V-EDTA complex depends on the solution pH as follows.

$VO_2(EDTA)^{3-}$ is formed at weak acid solutions, $VO_2H(EDTA)^{2-}$ is formed when acidic solutions have a pH under 3.5 and vanadates are formed in alkaline solutions [26].

Thus, due to the negative charge of the V-EDTA complex and surface charge of the NAC, the vanadium recovery percentage is increased at a low pH. This effect is demonstrated in Figs. 6(b) and (c).

As was mentioned earlier, the L/M ratio represents the EDTA concentration in the solution. The V-EDTA is a 1:1 complex, meaning that to form a mole of V-EDTA complex,

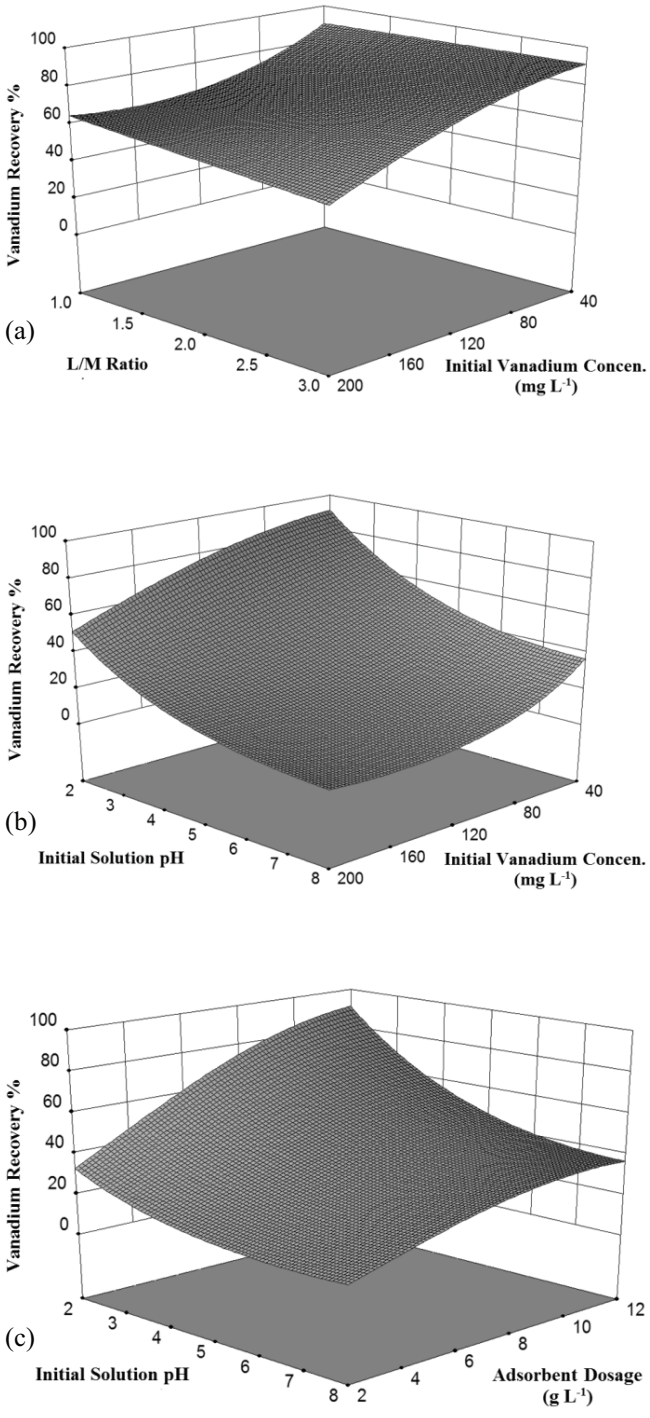

Fig. 6. 3D surface response for V-EDTA recovery with NAC vs. (a) L/M and initial vanadium concentration at pH_i = 2 and $C_{Ads.}$ = 12 g L^{-1}, (b) initial solution pH and initial vanadium concentration at L/M = 3 and $C_{Ads.}$ = 12 g L^{-1} and (c) initial solution pH and adsorbent dosage at $C_{i,V}$ = 40 mg L^{-1} and L/M = 3.

1 mol of vanadium and 1 mol of EDTA is required [26]. At L/M > 1, there is free EDTA in the solution that affects the adsorption process. Moreover, the species distribution of free EDTA depends on the solution pH as shown in Fig. 7 [39]. According to the perturbation plot (Fig. 5), the EDTA

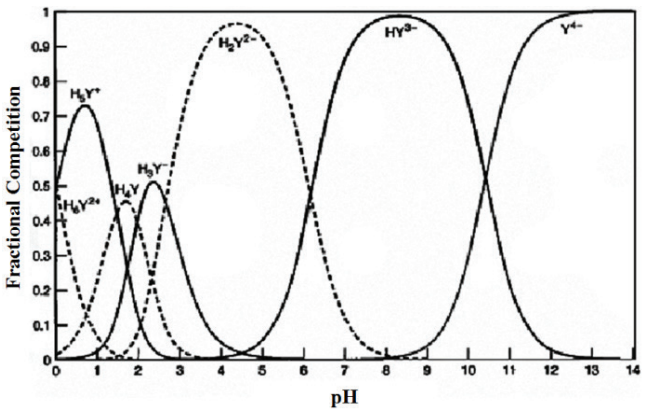

Fig. 7. pH effect on EDTA (Y) species in an aqueous solution ($C_{i,EDTA}$ = 10 mM) [39].

existence in the solution did not have much effect on V-EDTA adsorption, and there was NAC selectivity in the V-EDTA complex recovery. The following outlines the reasoning.

With the pH between 6 and 8, the dominant forms of V-EDTA complex and free EDTA are $VO_2(EDTA)^{3-}$ and $H(EDTA)^{3-}$, respectively. Both of them possess the same charge and will adsorb unselectively. However, based on the not too strong NAC surface charge at the current operating pH, the adsorption amounts of V-EDTA and free EDTA were low.

When the pH was decreased and maintained within 3–6, the free EDTA dominant species was $H_2(EDTA)^{2-}$, while the V-EDTA species was still $VO_2(EDTA)^{3-}$. Due to the NAC positive surface charge and the difference in ion charges, a selective adsorption between the V-EDTA complex and free EDTA took place.

At lower pH (2–3), the free EDTA species were $H_3(EDTA)^-$ and $H_4(EDTA)$, but the dominant species of the V-EDTA complex was $VO_2H(EDTA)^{2-}$ that still had greater charge in comparison with the free EDTA species. Therefore, there was selective adsorption of the V-EDTA complex, and the V-EDTA recovery increased substantially, as is displayed in Figs. 6(b) and (c).

According to the perturbation plot (Fig. 5), a slight increase in vanadium recovery percentage is obvious when the L/M ratio was increased from 1 to 3. This can be explained by the existence of free EDTA that will keep the solution pH at low values, and prevent it from increasing intensively. Thus, the V-EDTA recovery occurs slightly better at L/M = 3.

3.4. Parameter optimization

A numerical optimization by RSM software was performed on the operating parameters in order to achieve the highest vanadium recovery percentage. The optimization method scans the design space using the obtained model, to find one or more points at which the defined objective has been realized. In this step, the maximization of vanadium recovery percentage was selected as the objective for the Design Expert optimization module. Also, the "in range" criterion was selected for operating parameters. Finally, the maximum recovery percentage and the corresponding values of its operating factors were calculated by scanning the design space.

Table 6
Vanadium adsorption results by different adsorbents

Adsorbent	Recovery percentage	Adsorption capacity (mg g^{-1})	Initial V concentration (mg L^{-1})	L/M	pH	Adsorbent dosage (g L^{-1})	Reference
Modified tamarind fruit shell	–	45.9	5.0–50.0	–	2.0–8.0	0.5–5.0	[54]
Fe(III)/Cr(III) hydroxide waste	–	11.4	10.0–40.0	–	4.0	10.0	[55]
Mg/Al vanadate hydrotalcite	–	230.0	50.0	–	2.0–9.0	0.2	[38]
Waste metal sludge	–	24.8	7.6–48.4	–	–	10.0	[56]
Commercial activated carbon (CAC)	–	37.8	25.0–200.0	–	4.5	1.0	[6]
Modified CAC with Fe	–	119.0	25.0–200.0	–	4.5	1.0	[6]
Protonated chitosan flakes	–	12.2	1.0–5.0	–	4.4–5.0	5.0	[9]
Natural bentonite	43.0	–	50.0–200.0	–	2.0–10.0	1.0–6.0	[18]
$ZnCl_2$ activated carbon	–	24.9	40.0–120.0	–	4.0–9.0	4.0	[57]
Crosslinked chitosan	–	6.3	–	–	4.0–4.5	0.6	[58]
NAC	91.2	17.7	40.0–200.0	1–3	2.0–8.0	2.0–12.0	This work

The predicted maximum vanadium recovery percentage was 91.18, and the corresponding values of the operating factors were $C_{i,V}$ = 40.00 mg L^{-1}, L/M = 3.00, pH_i = 2.00 and $C_{Ads.}$ = 12.00 g L^{-1}, with a desirability value of 0.927. The optimum values were verified by conducting repeated experiments at the optimum operating conditions with a relative error of only 2.26%.

As mentioned earlier, this paper is the first investigation of V-EDTA recovery by adsorption method. A comparison of the obtained results with other previous works is presented in Table 6. In this work, the maximum vanadium recovery percentage and adsorption capacity were 91.18 (predicted by the model) and 17.67 mg g^{-1} (predicted by the Langmuir isotherm) at 25°C, respectively. It should be noted that the presence of free EDTA in the solution, reduced the adsorption capacity of vanadium in comparison with other works, in which only vanadium ions were adsorbed. However, the adsorption capacity obtained by the approach in this work was in reasonable agreement with other studies.

3.5. Adsorption kinetics

The V-EDTA adsorption kinetics was investigated to identify the adsorption mechanism and rate controlling process. Generally, in an adsorption process, both the reaction and mass transfer mechanisms influence the process. The reaction mechanism could be physical or chemical, and the mass transfer mechanism could be controlled by film resistance (external diffusion) or intra-particle resistance (internal diffusion) [6].

The effect of contact time on vanadium adsorption on NAC is presented in Fig. 8. The initial minutes of the adsorption process show that the rate of V-EDTA adsorption is relatively high due to the high driving force and fresh adsorbent. Accordingly, half of the total vanadium was adsorbed in about 120 min. In order to analyze these experimental data, four common kinetic models including pseudo-first-order [40], pseudo-second-order [41], intra-particle diffusion [42] and Boyd [6] were applied. The linear forms of these models are shown in Table 7.

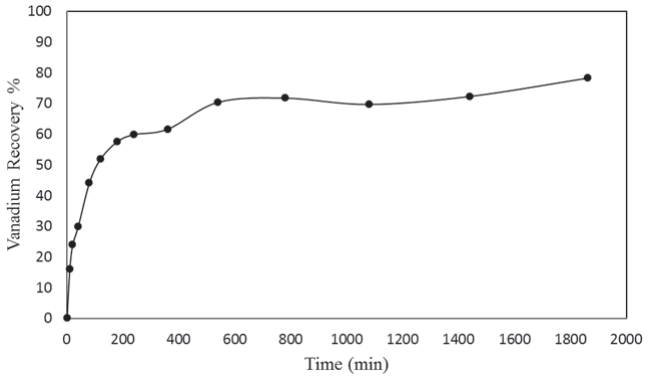

Fig. 8. Effect of contact time (min) on V-EDTA adsorption on NAC.

The experimental data were analyzed with the linear form of the abovementioned models, and the results are summarized in Table 7. According to the R^2 values, the pseudo-second-order kinetic model describes the experimental data very well compared with other kinetic models. Also, the equilibrium q predicted by this model is very close to the experimental value with a mere relative error of only 0.5%. It could be concluded that the pseudo-second-order model is validated, and that chemisorption (electrostatic attraction) may probably control the V-EDTA complex adsorption on NAC [43].

According to intra-particle diffusion model parameters (Table 7), the C parameter is not equal to zero and it shows that the fitted model does not pass through the origin, and has an intercept. Also, the obtained R^2 value was 0.78, which indicates the model's lack of fit. Therefore, the intra-particle diffusion is not a rate controlling mechanism of V-EDTA adsorption.

The Boyd kinetic model was applied to determine the rate-controlling step between film diffusion and intra-particle diffusion, and certify the results obtained from the intra-particle diffusion model. It can be seen in Fig. 9, that the data does not follow a linear form, and does not pass through the

Table 7
Linear forms and parameters of kinetic models for V-EDTA recovery[a]

Kinetic model	Linear form	Parameter	Value
Experimental q_e (mg g^{-1})			13.0299
Pseudo-first-order	$\ln(q_e - q_t) = \ln q_e - k_1 t$	k_1 (min^{-1})	0.0016
		q_e (mg g^{-1})	6.0646
		R^2	0.76
Pseudo-second-order	$\frac{t}{q_t} = \frac{1}{k_2 q_e^2} + \frac{1}{q_e} t$	k_2 (g mg^{-1} min^{-1})	0.0012
		q_e (mg g^{-1})	12.9703
		R^2	1.00
Intra-particle diffusion	$q_t = k_{diff} t^{0.5} + C$	k_{diff} (mg g^{-1} min$^{-0.5}$)	0.2260
		C (mg g^{-1})	4.7634
		R^2	0.78
Boyd	$-0.4977 - \ln(1 - F) = Bt$	B (min^{-1})	0.0016
		Intercept	0.2671
	$F = \frac{q_t}{q_e}$		
		R^2	0.76
	$B = \frac{\pi^2 D_e}{r^2}$		

[a]Each parameter description is reported in Symbols section.

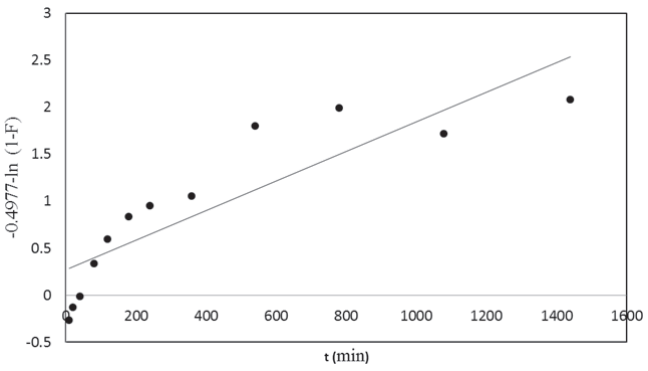

Fig. 9. Experimental data validation of Boyd model's linear form.

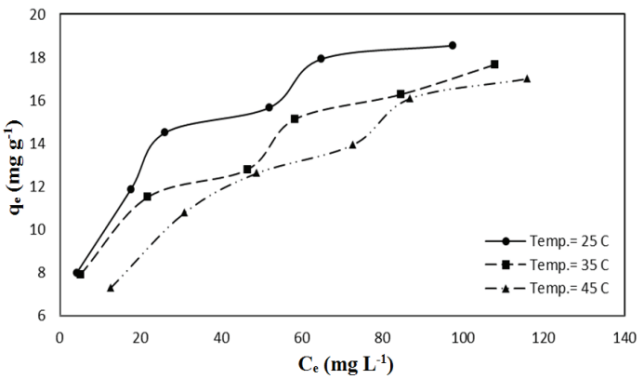

Fig. 10. V-EDTA adsorption isotherms on NAC at various temperatures.

origin. Therefore, it is concluded that the adsorption process is controlled more by film diffusion.

3.6. Adsorption isotherms

Equilibrium studies were carried out to identify NAC performance at different temperatures, different initial vanadium concentrations, and to find out the interaction of metal complex on NAC surface [44,45]. The V-EDTA adsorption isotherms at three temperatures are illustrated in Fig. 10. As can be seen, the adsorbed amount decreases by increasing the temperature, and the adsorption process may be exothermic. Non-linear Sips isotherm [46] and four linear isotherms including Langmuir [47], Freundlich [48], Temkin [49] and Dubinin–Radushkevich [50] were investigated to describe the experimental data. These isotherms are listed in Table 8.

At the empirical Langmuir isotherm, monolayer adsorption and equal energy of all active sites were used without considering the interaction between the adsorbed component and adsorbent [47]. However, the Freundlich isotherm has the ability to describe the adsorption at the multilayer heterogeneous surface [51]. Also, unlike the Langmuir isotherm, the Freundlich isotherm assumes that there are active sites, which have been occupied earlier due to their stronger energy [52]. The Sips isotherm that describes the physical and chemical characterization of the adsorption process is obtained by hybridizing the Langmuir and Freundlich isotherms [46].

The adsorption behavior of the V-EDTA complex on NAC was investigated by incorporating the dimensionless and constant separation factor (R_L) that is represented in Eq. (10). If $0 < R_L < 1$, the adsorption process is favorable, $R_L > 1$ indicates an unfavorable adsorption, $R_L = 1$ indicates a linear process and $R_L = 0$ represents an irreversible adsorption process [53].

$$R_L = \frac{1}{1 + K_L C_{i,V}} \tag{10}$$

The Dubinin–Radushkevich isotherm is useful to identify whether the adsorption has a physical or chemisorption (electrostatic attraction) nature. The parameter E (J mol^{-1}), expresses the free energy required, when 1 mol of adsorbate is moved from the bulk of the solution to the surface of the adsorbent (Eq. (11)). If the E magnitude is less than 8 kJ mol^{-1}, the adsorption process is physical. Otherwise, if 8 kJ mol^{-1} < E < 16 kJ mol^{-1}, it can then be deducted that the process has a chemical nature and is affected by electrostatic forces [50].

$$E = \frac{1}{(2\beta)^{1/2}} \tag{11}$$

Table 8
Isotherm equations[a]

Isotherm	Equation
Langmuir	$\frac{1}{q_e} = \frac{1}{q_{\max} K_L} \times \frac{1}{C_e} + \frac{1}{q_{\max}}$
Freundlich	$\log q_e = \frac{1}{n} \log C_e + \log K_F$
Sips	$q_e = \frac{Q_s K_s C_e^m}{1 + K_s C_e^m}$
Temkin	$q_e = B \ln K_T + B \ln C_e$
Dubinin–Radushkevich	$\ln q_e = \ln q_m - \beta\varepsilon^2$
	$\varepsilon = RT \ln\left(1 + \frac{1}{C_e}\right)$

[a]Each parameter description is reported in Symbols section.

The Temkin isotherm states that by covering the adsorbent's surface at the middle concentrations of the adsorbate, the adsorption heat will follow a linear decreasing pattern instead of a logarithmic one for all the adsorbate molecules in the layer [49].

The parameters and constants of the isotherm models are reported in Table 9. The R^2 values indicate, that the Freundlich and Dubinin–Radushkevich isotherms describe the experimental data better than other isotherms at all investigated temperatures. According to Langmuir isotherm constants, the predicted maximum adsorption capacity (q_{max}) for vanadium recovery on NAC was 17.670 mg g^{-1} at 25°C. Also, the R_L values were in the range of 0–1 at all temperatures. This indicates that the V-EDTA complex adsorption on NAC was favorable. This favorability is proved by the Freundlich isotherm exponent, for which 1/n values are in the range of 0–1 and this also indicates a successful recovery of V-EDTA from the solution.

It can be concluded from the parameter analysis of Temkin isotherm (Table 9), that the adsorption heat may follow a linear form, when the NAC surface is covered. The E parameters calculated from Dubinin–Radushkevich constants demonstrate that the V-EDTA adsorption on NAC followed a chemical pattern (electrostatic attraction) and it proves the validity of the pseudo-second-order kinetic model and the corresponding obtained results.

3.7. Thermodynamic parameters

The Langmuir constant, K_L (L mol^{-1}), was used to determine the thermodynamic parameters including $\Delta G°$ (kJ mol^{-1}), $\Delta H°$ (kJ mol^{-1}) and $\Delta S°$ (kJ mol^{-1} K^{-1}) that represent changes in free energy, enthalpy and entropy, respectively. By considering Eq. (13) and its corresponding plot (Fig. 11), $\Delta H°$ and $\Delta S°$ can be calculated, and $\Delta G°$ is obtained from Eqs. (12) and (14) [6].

Table 9
Parameters of isotherm models for V-EDTA adsorption on NAC

Isotherm	Parameter	Temperature (K)		
		298	308	318
Langmuir	K_L (L mol^{-1})	9,701.220	9,317.603	2,545.879
	q_{max} (mg g^{-1})	17.670	16.070	18.557
	R_L	0.016–0.050	0.017–0.052	0.059–0.167
	R^2	0.95	0.92	0.98
Freundlich	n	3.648	3.860	2.615
	K_F (mg$^{1-(1/n)}$ L$^{1/n}$ g^{-1})	5.499	5.124	2.815
	R^2	0.98	0.98	0.99
Sips	Q_s (mg g^{-1})	33.0852	40.000	52.746
	K_s (L^n mg^{-n})	0.164	0.123	0.047
	m	0.453	0.386	0.489
	R^2	0.98	0.96	0.99
Temkin	K_T (L g^{-1})	2.236	2.117	0.391
	B (J mol^{-1})	3.446	3.097	4.383
	R^2	0.97	0.95	0.98
Dubinin–Radushkevich	β (mol^2 J^{-2})	2.844×10^{-9}	2.545×10^{-9}	3.794×10^{-9}
	q_m (mol g^{-1})	7.344×10^{-4}	6.245×10^{-4}	8.945×10^{-4}
	E (kJ mol^{-1})	13.260	14.018	11.479
	R^2	0.98	0.97	0.99

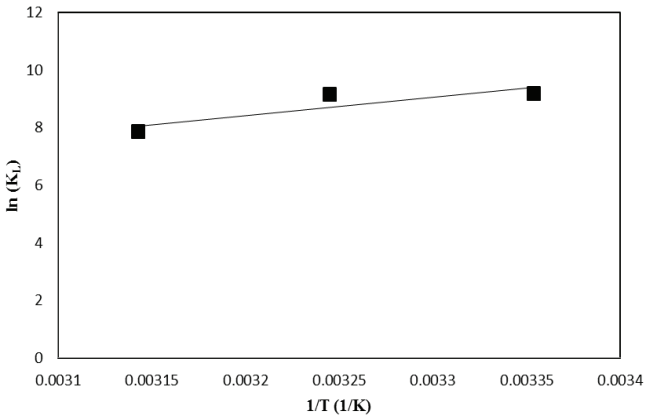

Fig. 11. Plot of $\ln(K_L)$ vs. $1/T$ for V-EDTA adsorption on NAC.

Table 10
Thermodynamic parameters of V-EDTA adsorption on NAC

Temperature (K)	$\Delta G°$ (kJ mol^{-1})	$\Delta H°$ (kJ mol^{-1})	$T\Delta S°$ (kJ mol^{-1})	$\Delta S°$ (kJ mol^{-1} K^{-1})
298	–22.756	–52.196	–29.440	–0.097
308	–23.415		–28.781	
318	–20.743		–31.435	

$$\Delta G° = -RT\ln(K_L) \tag{12}$$

$$\ln(K_L) = -\frac{\Delta H°}{RT} + \frac{\Delta S°}{R} \tag{13}$$

$$T\Delta S° = \Delta H° - \Delta G° \tag{14}$$

Table 10 represents the thermodynamic parameters obtained at different temperatures. The negative values of $\Delta G°$ and $\Delta H°$ indicate that the adsorption process occurs spontaneously, and the process is exothermic. Also, the negative value of $\Delta S°$ indicates that irregularities are decreasing at the adsorbent and solution intersections during the adsorption process.

3.8. Mechanism investigations

To study the adsorption mechanism, it was important to investigate the adsorption of other components in the solution such as free EDTA and Na cation, in order to determine the adsorbent efficiency and its selectivity on the V-EDTA complex.

3.8.1. Free EDTA adsorption

Due to the negative charge of free EDTA, its adsorption occurred during the vanadium recovery process. The adsorption investigation of this component was carried out by considering the central point of the marked RSM star points in Table 4 as the reference point. Fig. 12 represents the free

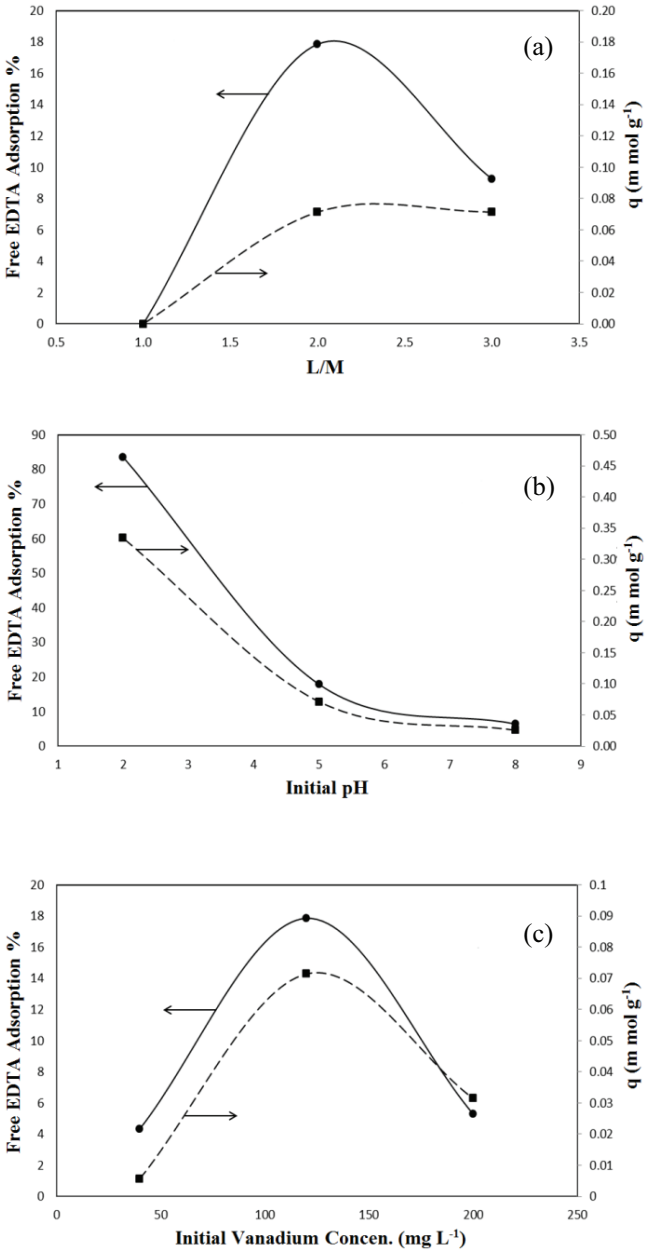

Fig. 12. Free EDTA adsorption vs. (a) L/M ($C_{i,V}$, pH_i and $C_{Ads.}$ = RSM CP), (b) pH_i ($C_{i,V}$, L/M and $C_{Ads.}$ = RSM CP) and (c) $C_{i,V}$ (L/M, pH_i and $C_{Ads.}$ = RSM CP).

EDTA adsorption percentage and the amount adsorbed (q) on NAC.

At L/M = 1, there was no free EDTA in the solution, so the free EDTA adsorption amount is zero in Fig. 12(a). By increasing the L/M ratio, free EDTA will exist in the solution and its adsorption occurs until the NAC active sites are occupied. From this point at L/M > 2, there is no ability to adsorb free EDTA, and as a result, the amount of adsorbed (q) remains constant and the adsorption percentage decreases.

As is shown in Fig. 12(b), at initial pH = 8, a small amount of free EDTA was adsorbed (6.43% and 0.026 mmol g^{-1}). Since the free EDTA form was $H(EDTA)^{3-}$ at this pH, the positive charge of NAC adsorbent was negligible, and there was not

sufficient adsorption driving force. However, by reducing the pH, the positive surface charge of NAC became stronger, and as a result, the free EDTA adsorption increased substantially until the initial pH = 2. The adsorption percentage and the amount of EDTA adsorbed were 83.57% and 0.334 mmol g^{-1}, respectively.

The free EDTA concentration in the solution also increases by keeping the L/M ratio constant and increasing the initial vanadium concentration. By increasing the initial vanadium concentration from 40 to 120 mg L^{-1}, its adsorption increases from 4.35% to 17.86%, (Fig. 12(c)) due to an increase in the free EDTA driving force. However, selective adsorption will take place between the V-EDTA complex and free EDTA within a range of 120–200 mg L^{-1} of vanadium. The free EDTA adsorption decreased due to dominant charges of V-EDTA complex and free EDTA (that were 3 and 2 at the central point pH), as well as the higher V-EDTA driving force sustained by its concentration. Finally, at vanadium concentration of 200 mg L^{-1}, 5.29% and 0.031 mmol g^{-1} of EDTA was adsorbed as illustrated in Fig. 12(c).

3.8.2. Na adsorption

The star point concept was also applied for Na adsorption investigation, similar to the free EDTA adsorption approach. However, it was not possible to investigate Na adsorption at the initial pH of the solutions, until a NaOH solution was used to adjust the pH. The results of Na adsorption studies are shown in Fig. 13. There is no tendency to adsorb Na based on positive charge of Na in the solution and NAC positive surface charge at the operating pH (2–8), even though the adsorption of small amounts of Na unavoidable.

Fig. 13(a) represents the Na adsorption with varied L/M. By increasing the L/M ratio, Na concentration increases and its adsorption percentage decreases based on lack of NAC tendency to adsorb Na. However, the amount of Na adsorbed per unit mass of NAC (q) increases slightly when the increasing of the L/M ratio increases the driving force, which leads to a slightly higher amount of Na adsorbed on NAC. The maximum Na adsorption percentage in Fig. 13(a) was 2.62% at L/M = 1, and the maximum amount adsorbed was 0.901 mg g^{-1} at L/M = 3.

The same mechanism occurred while the initial concentration of vanadium was varied. This effect is shown in Fig. 13(b). It shows that by increasing the initial vanadium concentration, the Na concentration also increases, and as a result, the adsorption percentage decreases and the amount of Na adsorbed increases slightly. The maximum Na adsorption percentage and the amount of Na adsorbed were 3.47% and 0.970 mg g^{-1}, respectively, at the initial vanadium concentration of 40 and 200 mg L^{-1}.

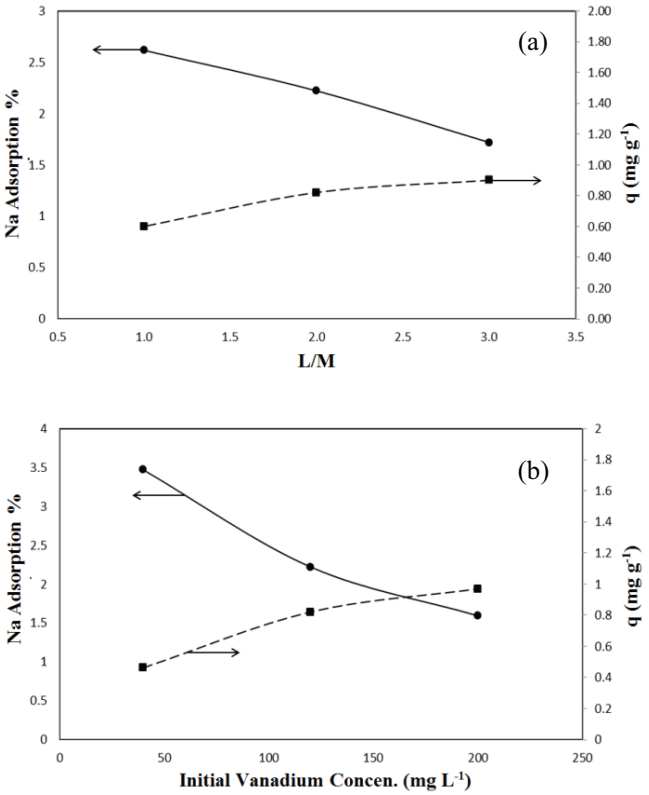

Fig. 13. Na adsorption vs. (a) L/M ($C_{i,V}$, pH_i and $C_{Ads.}$ = RSM CP) and (b) $C_{i,V}$ (L/M, pH_i and $C_{Ads.}$ = RSM CP).

4. Conclusion

In this paper, the optimization of V-EDTA adsorption from an aqueous phase on a commercial activated carbon was investigated. The investigation was carried out by RSM, and a proper non-complete cubic model was offered. The obtained results validated the appropriate ability of Norit activated carbon (NAC) to adsorb the V-EDTA complex. A parameter optimization was performed by solving the regression model, and the maximum predicted vanadium recovery percentage was 91.18 with a relative error of 2.26%. The optimum conditions were: initial vanadium concentration = 40 mg L^{-1}, molar ratio of EDTA to vanadium = 3, initial solution pH = 2 and adsorbent dosage = 12 g L^{-1} after a 4 h contact time. The final model quality and accuracy were assessed by employing model statics and diagnostic plots. The pseudo-second-order kinetic model and both the Freundlich and Dubinin–Radushkevich isotherms were fitted to the kinetic and equilibrium data, respectively. The kinetic and equilibrium results indicated that the V-EDTA adsorption on NAC was controlled by a chemisorption mechanism, and it was spontaneous, exothermic and feasible. The results of Na and free EDTA adsorption studies to investigate the recovery process mechanism showed that Na adsorption is negligible, but the free EDTA adsorption was relatively high at operating pH = 2. Also, this work could be a preliminary study to develop a cyclic vanadium extraction process from secondary resources.

Symbols

B — Temkin isotherm constant related to the heat of adsorption, J mol^{-1}
C — Intra-particle intercept, mg g^{-1}
C_e — Vanadium concentration at equilibrium, mg L^{-1}, mol L^{-1}
D_e — Effective diffusion coefficient of Boyd kinetic model, m^2 s^{-1}
k_1 — Rate constant of pseudo-first-order kinetic model, min^{-1}

k_2 — Rate constant of pseudo-second-order kinetic model, g mg^{-1} min^{-1}
k_{diff} — Rate constant of intra-particle diffusion kinetic model, mg g^{-1} $min^{-1/2}$
K_F — Freundlich isotherm constant related to adsorption capacity of NAC, $mg^{1-(1/n)}$ $L^{1/n}$ g^{-1}
K_L — Langmuir isotherm constant related to energy of adsorption, L mol^{-1}
K_s — Sips isotherm equilibrium constant, L^n mg^{-n}
K_T — Equilibrium binding constant related to the maximum binding energy, L mg^{-1}
m — Sips isotherm exponent
n — Freundlich isotherm exponent related to adsorption intensity
q_e — Amount of vanadium adsorbed per unit weight of NAC at equilibrium, mg g^{-1}
q_m — Theoretical saturation capacity, mol g^{-1}
q_{max} — Maximum adsorption capacity of NAC, mg g^{-1}
q_t — Amount of vanadium adsorbed per unit weight of NAC at time t, mg g^{-1}
Q_s — Sips isotherm constant related to adsorption capacity, mg g^{-1}
r — Radius of the NAC particles, m
R — Universal gas constant, 8.314 J mol^{-1} K^{-1}
t — Time, min
T — Temperature, K
β — Dubinin–Radushkevich constant term related to the mean free energy of adsorption per mole of the adsorbate, mol^2 J^{-2}
ε — Dubinin–Radushkevich Polanyi potential related to the equilibrium concentration, J mol^{-1}

References

[1] M.N. Alyemeni, I. Almohisen, Effect of anthropogenic activities on accumulation of heavy metals in legumes crops, Riyadh, Saudi Arabia, APCBEE Procedia, 10 (2014) 275–280.
[2] C. Luo, C. Liu, Y. Wang, X. Liu, F. Li, G. Zhang, X. Li, Heavy metal contamination in soils and vegetables near an e-waste processing site, south China, J. Hazard. Mater., 186 (2011) 481–490.
[3] Q. Wu, Y. Cui, Q. Li, J. Sun, Effective removal of heavy metals from industrial sludge with the aid of a biodegradable chelating ligand GLDA, J. Hazard. Mater., 283 (2015) 748–754.
[4] C. Alonso-Hernández, J. Bernal-Castillo, Y. Bolanos-Alvarez, M. Gómez-Batista, M. Diaz-Asencio, Heavy metal content of bottom ashes from a fuel oil power plant and oil refinery in Cuba, Fuel, 90 (2011) 2820–2823.
[5] H. Wyers, Some toxic effects of vanadium pentoxide, Br. J. Ind. Med., 3 (1946) 177–182.
[6] H. Sharififard, M. Soleimani, Performance comparison of activated carbon and ferric oxide-hydroxide–activated carbon nanocomposite as vanadium(V) ion adsorbents, RSC Adv., 5 (2015) 80650–80660.
[7] G.T. Whiting, J.K. Bartley, N.F. Dummer, G.J. Hutchings, S.H. Taylor, Vanadium promoted molybdenum phosphate catalysts for the vapour phase partial oxidation of methanol to formaldehyde, Appl. Catal., A, 485 (2014) 51–57.
[8] Z. Yuan, X. Li, Y. Duan, Y. Zhao, H. Zhang, Application and degradation mechanism of polyoxadiazole based membrane for vanadium flow batteries, J. Membr. Sci., 488 (2015) 194–202.
[9] A. Padilla-Rodríguez, J.A. Hernández-Viezcas, J.R. Peralta-Videa, J.L. Gardea-Torresdey, O. Perales-Pérez, F.R. Román-Velázquez, Synthesis of protonated chitosan flakes for the removal of vanadium(III, IV and V) oxyanions from aqueous solutions, Microchem. J., 118 (2015) 1–11.
[10] M.F. Ali, S. Abbas, A review of methods for the demetallization of residual fuel oils, Fuel Process. Technol., 87 (2006) 573–584.
[11] S. Ramírez, P. Schacht, R. Quintana-Solórzano, J. Aguilar, Leaching of heavy metals under ambient resembling conditions from hydrotreating spent catalysts, Fuel, 110 (2013) 286–292.
[12] Z. Zhao, M. Guo, M. Zhang, Extraction of molybdenum and vanadium from the spent diesel exhaust catalyst by ammonia leaching method, J. Hazard. Mater., 286 (2015) 402–409.
[13] L. Zeng, C.Y. Cheng, A literature review of the recovery of molybdenum and vanadium from spent hydrodesulphurisation catalysts: part II: separation and purification, Hydrometallurgy, 98 (2009) 10–20.
[14] M.A. Al-Ghouti, Y.S. Al-Degs, A. Ghrair, H. Khoury, M. Ziedan, Extraction and separation of vanadium and nickel from fly ash produced in heavy fuel power plants, Chem. Eng. J., 173 (2011) 191–197.
[15] I.S. Pinto, H.M. Soares, Microwave-assisted selective leaching of nickel from spent hydrodesulphurization catalyst: a comparative study between sulphuric and organic acids, Hydrometallurgy, 140 (2013) 20–27.
[16] S. Goel, K. Pant, K. Nigam, Extraction of nickel from spent catalyst using fresh and recovered EDTA, J. Hazard. Mater., 171 (2009) 253–261.
[17] S.E. Bailey, T.J. Olin, R.M. Bricka, D.D. Adrian, A review of potentially low-cost sorbents for heavy metals, Water Res., 33 (1999) 2469–2479.
[18] A. Etaati, M. Soleimani, Optimizing of vanadium adsorption onto natural bentonite using response surface methodology, Int. J. Chem. Environ. Eng., 6 (2015) 357–361.
[19] H. Sharififard, M. Soleimani, Modeling and experimental study of vanadium adsorption by iron-nanoparticle-impregnated activated carbon, Res. Chem. Intermed., 43 (2017) 2501–2516.
[20] M. Kavand, T. Kaghazchi, M. Soleimani, Optimization of parameters for competitive adsorption of heavy metal ions (Pb^{2+}, Ni^{2+}, Cd^{2+}) onto activated carbon, Korean J. Chem. Eng., 31 (2014) 692–700.
[21] H. Sharififard, F. Zokaee Ashtiani, M. Soleimani, Adsorption of palladium and platinum from aqueous solutions by chitosan and activated carbon coated with chitosan, Asia-Pac. J. Chem. Eng., 8 (2013) 384–395.
[22] M. Barkat, D. Nibou, S. Chegrouche, A. Mellah, Kinetics and thermodynamics studies of chromium(VI) ions adsorption onto activated carbon from aqueous solutions, Chem. Eng. Process., 48 (2009) 38–47.
[23] N. Asasian, T. Kaghazchi, M. Soleimani, Elimination of mercury by adsorption onto activated carbon prepared from the biomass material, J. Ind. Eng. Chem., 18 (2012) 283–289.
[24] S. Brunauer, P.H. Emmett, E. Teller, Adsorption of gases in multimolecular layers, J. Am. Chem. Soc., 60 (1938) 309–319.
[25] S.A. Dastgheib, D.A. Rockstraw, A model for the adsorption of single metal ion solutes in aqueous solution onto activated carbon produced from pecan shells, Carbon, 40 (2002) 1843–1851.
[26] A. Ringbom, S. Siitonen, B. Skrifvars, The ethylenediaminetetraacetate complexes of vanadium(V), Acta Chem. Scand., 11 (1957) 10.
[27] H.-s. Zhu, X.-j. Yang, Y.-p. Mao, Y. Chen, X.-l. Long, W.-k. Yuan, Adsorption of EDTA on activated carbon from aqueous solutions, J. Hazard. Mater., 185 (2011) 951–957.
[28] D.C. Montgomery, Design and Analysis of Experiments, John Wiley & Sons, Hoboken, 2008.
[29] M.J. Bashir, H.A. Aziz, M.S. Yusoff, M.N. Adlan, Application of response surface methodology (RSM) for optimization of ammoniacal nitrogen removal from semi-aerobic landfill leachate using ion exchange resin, Desalination, 254 (2010) 154–161.
[30] U.K. Garg, M. Kaur, V. Garg, D. Sud, Removal of nickel (II) from aqueous solution by adsorption on agricultural waste biomass using a response surface methodological approach, Bioresour. Technol., 99 (2008) 1325–1331.
[31] N. Mehrabi, M. Soleimani, M.M. Yeganeh, H. Sharififard, Parameter optimization for nitrate removal from water using activated carbon and composite of activated carbon and Fe_2O_3 nanoparticles, RSC Adv., 5 (2015) 51470–51482.

[32] M. Amini, H. Younesi, N. Bahramifar, A.A.Z. Lorestani, F. Ghorbani, A. Daneshi, M. Sharifzadeh, Application of response surface methodology for optimization of lead biosorption in an aqueous solution by *Aspergillus niger*, J. Hazard. Mater., 154 (2008) 694–702.
[33] M. Kavand, M. Soleimani, T. Kaghazchi, N. Asasian, Competitive separation of lead, cadmium, and nickel from aqueous solutions using activated carbon: response surface modeling, equilibrium, and thermodynamic studies, Chem. Eng. Commun., 203 (2016) 123–135.
[34] D.L. Pavia, G.M. Lampman, G.S. Kriz, J.A. Vyvyan, Introduction to Spectroscopy, Cengage Learning, Stamford, 2014.
[35] K.Y. Nandiwale, N.D. Galande, V.V. Bokade, Process optimization by response surface methodology for transesterification of renewable ethyl acetate to butyl acetate biofuel additive over borated USY zeolite, RSC Adv., 5 (2015) 17109–17116.
[36] M.R. Hormozi-Nezhad, M. Jalali-Heravi, H. Robatjazi, H. Ebrahimi-Najafabadi, Controlling aspect ratio of colloidal silver nanorods using response surface methodology, Colloids Surf., A, 393 (2012) 46–52.
[37] T. Ölmez, The optimization of Cr(VI) reduction and removal by electrocoagulation using response surface methodology, J. Hazard. Mater., 162 (2009) 1371–1378.
[38] T. Wang, Z. Cheng, B. Wang, W. Ma, The influence of vanadate in calcined Mg/Al hydrotalcite synthesis on adsorption of vanadium (V) from aqueous solution, Chem. Eng. J., 181 (2012) 182–188.
[39] K. Zohdy, Surface protection of carbon steel in acidic solution using ethylenediaminetetraacetic disodium salt, Int. J. Electrochem. Sci., 10 (2015) 414–431.
[40] H. Yuh-Shan, Citation review of Lagergren kinetic rate equation on adsorption reactions, Scientometrics, 59 (2004) 171–177.
[41] Y.-S. Ho, Second-order kinetic model for the sorption of cadmium onto tree fern: a comparison of linear and non-linear methods, Water Res., 40 (2006) 119–125.
[42] W.J. Weber, J.C. Morris, Kinetics of adsorption on carbon from solution, J. Sanit. Eng. Div., 89 (1963) 31–60.
[43] Y.-S. Ho, G. McKay, Pseudo-second order model for sorption processes, Process Biochem., 34 (1999) 451–465.
[44] S. Rangabhashiyam, N. Anu, M.G. Nandagopal, N. Selvaraju, Relevance of isotherm models in biosorption of pollutants by agricultural byproducts, J. Environ. Chem. Eng., 2 (2014) 398–414.
[45] U. Etim, S. Umoren, U. Eduok, Coconut coir dust as a low cost adsorbent for the removal of cationic dye from aqueous solution, J. Saudi Chem. Soc., 20 (2016) S67–S76.
[46] Y. Liu, Y.-J. Liu, Biosorption isotherms, kinetics and thermodynamics, Sep. Purif. Technol., 61 (2008) 229–242.
[47] I. Langmuir, The constitution of solids and liquids part I. solids, J. Am. Chem. Soc., 38 (1916) 2221–2295.
[48] Y. Yu, X. Liu, W. Gong, G. Liu, D. Cheng, H. Bao, D. Gao, Adsorption of potentially toxic metals on negatively charged liposomes: equilibrium isotherms and quantitative modeling, RSC Adv., 4 (2014) 42591–42597.
[49] G.S. ElShafei, I. Nasr, A.S. Hassan, S. Mohammad, Kinetics and thermodynamics of adsorption of cadusafos on soils, J. Hazard. Mater., 172 (2009) 1608–1616.
[50] C. Wang, J. Ni, J. Zhou, J. Wen, X. Lü, Strategically designed porous polysilicate acid/graphene composites with wide pore size for methylene blue removal, RSC Adv., 3 (2013) 23139–23145.
[51] A. Heidari, H. Younesi, Z. Mehraban, H. Heikkinen, Selective adsorption of Pb(II), Cd(II), and Ni(II) ions from aqueous solution using chitosan–MAA nanoparticles, Int. J. Biol. Macromol., 61 (2013) 251–263.
[52] I. Tan, A. Ahmad, B. Hameed, Adsorption isotherms, kinetics, thermodynamics and desorption studies of 2,4,6-trichlorophenol on oil palm empty fruit bunch-based activated carbon, J. Hazard. Mater., 164 (2009) 473–482.
[53] K. Hall, L. Eagleton, A. Acrivos, T. Vermeulen, Pore- and solid-diffusion kinetics in fixed-bed adsorption under constant-pattern conditions, Ind. Eng. Chem. Fundam., 5 (1966) 212–223.
[54] T. Anirudhan, P. Radhakrishnan, Adsorptive performance of an amine-functionalized poly(hydroxyethylmethacrylate)-grafted tamarind fruit shell for vanadium(V) removal from aqueous solutions, Chem. Eng. J., 165 (2010) 142–150.
[55] K. Prathap, C. Namasivayam, Adsorption of vanadate (V) on Fe (III)/Cr (III) hydroxide waste, Environ. Chem. Lett., 8 (2010) 363–371.
[56] A. Bhatnagar, A.K. Minocha, D. Pudasainee, H.-K. Chung, S.-H. Kim, H.-S. Kim, G. Lee, B. Min, B.-H. Jeon, Vanadium removal from water by waste metal sludge and cement immobilization, Chem. Eng. J., 144 (2008) 197–204.
[57] C. Namasivayam, D. Sangeetha, Removal and recovery of vanadium(V) by adsorption onto $ZnCl_2$ activated carbon: kinetics and isotherms, Adsorption, 12 (2006) 103–117.
[58] S. Qian, H. Wang, G. Huang, S. Mo, W. Wei, Studies of adsorption properties of crosslinked chitosan for vanadium(V), tungsten(VI), J. Appl. Polym. Sci., 92 (2004) 1584–1588.